Analysis of the spectral function of $Nd_{1.85}Ce_{0.15}CuO_4$ obtained by angle-resolved photoemission spectroscopy

F. Schmitt,[1] W. S. Lee,[1] D.-H. Lu,[2] W. Meevasana,[3] E. Motoyama,[1] M. Greven,[1,2] and Z.-X. Shen[1,2,3]

[1]*Department of Applied Physics, Stanford University, Stanford, California 94305, USA*

[2]*Stanford Synchrotron Radiation Laboratory, Menlo Park, California 94025, USA*

[3]*Department of Physics, Stanford University, Stanford, California 94305, USA*

Samples of $Nd_{2-x}Ce_xCuO_4$, an electron-doped high-temperature superconducting cuprate, near optimal doping at $x=0.155$ were measured via angle-resolved photoemission. We report a renormalization feature in the self-energy ("kink") in the band dispersion at $\approx 50-60$ meV present in nodal and antinodal cuts across the Fermi surface. Specifically, while the kink had been seen in the antinodal region, it is now observed also in the nodal region, reminiscent of what has been observed in hole-doped cuprates.

The high-temperature superconducting cuprates (HTSCs) have received much attention since their discovery, as the mechanism of their unusually high critical temperatures remains yet to be determined. $Nd_{2-x}Ce_xCuO_4$ (NCCO) is a class of cuprates that resides on the relatively less-studied electron (n)-doped side of the phase diagram,[1] which is qualitatively different from the hole (p)-doped side. NCCO has recently been attracting increased interest,[2–9] in particular regarding its links to their more commonly studied hole-doped counterparts.[10]

Angle-resolved photoemission spectroscopy (ARPES) is used as a powerful direct probe of the electronic band structure (the one-particle spectral function).[10] Sudden changes in the slope in the band dispersion observed via ARPES allow one to infer the underlying physics causing these renormalizations.[10] Low-energy renormalizations have been prevalently found in the nodal region of p-doped cuprates via ARPES,[10,11] but not in the nodal region of n-doped cuprates,[5] casting doubt on the universality of the renormalization effect in the cuprates for the whole phase diagram.

In this Rapid Communication, we confirm a renormalization in NCCO near optimal doping ($x=0.155$) around 55 meV in the antinodal (X-M) region and report one in the nodal (Γ-M) region of about the same energy which was not observed earlier.[5] We do not observe any change of these renormalizations across the superconducting (SC) phase transition. These results suggest that an oxygen phonon mode with comparable energy scale is a likely origin of these renormalizations. In light of the presence of phononic coupling effects, one needs to carefully examine the data to separate the respective contributions to the low-energy spectra from AF band folding and lattice coupling effects, as the latter can also break the low-energy dispersion into two "branches."

ARPES data were taken at beamline 5–4 of the Stanford Synchrotron Radiation Laboratory with Scienta SES200 and R4000 analyzers at a photon energy of 16.75 eV. The a (b) axis was aligned at $45°$ to the light polarization for the nodal cut, and parallel to the light polarization for the other cuts. The energy resolution was ≈ 10 meV and the angular resolution $\approx 0.3°$. All samples were cleaved at pressures better than 3×10^{-11} Torr; the measurement temperature was 10 K unless otherwise specified. Single crystals of NCCO were

grown at Stanford University.[12] The doping level, determined by inductively coupled plasma spectroscopy, is $15.5\% \pm 0.7\%$ Ce. T_C was determined by superconducting quantum interference device magnetometry to be 25 K with a transition width of ≈ 2 K.

We show three different cuts through the Fermi surface (FS) in Fig. 1: one in the antinodal, one in the nodal, and one near the hot spot region [region of low intensity at E_F near the crossing of the FS with the antiferromagnetic (AF) Brillouin zone (BZ) boundary]. The insets in Figs. 1(a), 1(c), and 1(e) show the respective locations of the three cuts in the BZ relative to the FS of NCCO. The raw data of these three cuts, including their energy distribution curves (EDCs), are shown in Figs. 1(a)–1(f). Momentum distribution curve (MDC) analysis, i.e., a fit with a Lorentzian line shape, is used to extract Re Σ and Im Σ; Im Σ corresponds to the extracted width of the Lorentzian times the Fermi velocity, while Re Σ is obtained by subtracting the extracted position from an assumed bare band. Apart from the assumptions and details of this analysis,[5,13] we phenomenologically apply MDC/EDC spectral-function analysis as a tool for quantification, lacking a definitive theory.

The raw spectrum in Fig. 1(a) of the antinodal cut reveals a renormalization at about 50 meV binding energy. The corresponding EDC curves in Fig. 1(b) display a sharp quasiparticle peak near the E_F crossing. This peak terminates with a dip at about 50 meV binding energy. The linewidth decreases upon approaching E_F. To determine the self-energy, a parabolic bare band has been assumed and constructed by fixing the E_F-crossing point and the band bottom, which are determined by a linear fit to a MDC analysis <40 meV, and a parabolic fit to an EDC analysis ≥ 250 meV, respectively [cf. Figure 1(a)]. The band bottom thus obtained is at about 300 meV. The discrepancy between the EDC and MDC fitting around 250 meV shows the limits of both analyses.[10]

The raw spectrum of the nodal region cut depicted in Fig. 1(c) exhibits a similar renormalization feature at a similar energy of about 50 meV as seen in the antinodal region. The EDCs [Fig. 1(d)] show a peak at the E_F crossing. Again, the peak terminates at roughly 50 meV. A resemblance is found in the peak-dip-hump (PDH) structure seen over a wide temperature range in the nodal EDCs of the single-layer compound Bi2201 (Ref. 11) which is attributed to electron-
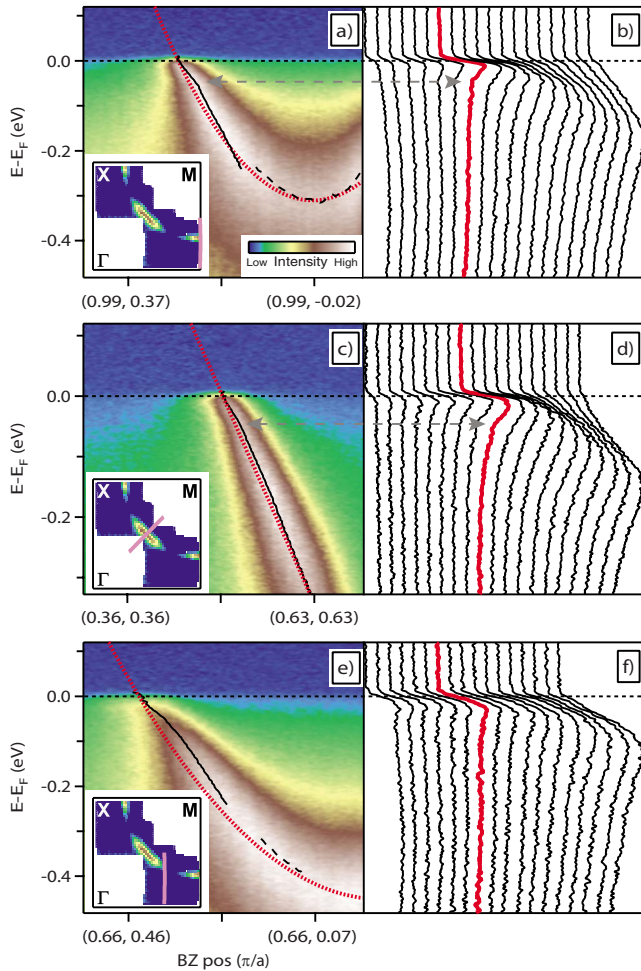
FIG. 1. (Color online) FS cuts and EDCs of the [(a), (b)] anti-nodal, [(c), (d)] nodal, and [(e), (f)] hot spot regions. The insets in (a), (c), and (e) depict a map of the upper right quadrant of the FS; the cut positions are indicated by pink (gray) lines. (a), (c), and (e) show the raw spectra, while (b), (d), and (f) show EDCs near the Fermi crossing of the respective raw spectra on the left. Also indicated in the raw spectra are the MDC fits in solid black, EDC fits in dashed black, and assumed bare band in dotted red (black). The EDCs in (b), (d), and (f) at E_F crossing are highlighted in thick red (black). A renormalization is seen in the nodal and antinodal regions around 50 meV (gray dashed arrows).

phonon interaction, although a hump is absent here in the antinodal and faint in the nodal cuts. The assumed linear bare band was modeled by connecting the E_F crossing point obtained by a linear fit to the MDC dispersion <40 meV, and a point at 300 meV obtained by a linear fit to the MDC dispersion between 250 and 330 meV [cf. Fig. 1(c)]. We note that assuming different bare bands changes the extracted renormalization strength, but not appreciably the energy of sharp features in the real part of the self-energy.

The spectrum of the hot spot region is displayed in Fig. 1(e). Since the hot spot is located on the AF BZ boundary, the low-energy physics and thus the kink will be influenced by a crossover of two bands that could originate from back-folding at the AF BZ boundary as we discuss later. Bare band assumption and construction are analogous to the antinodal region.
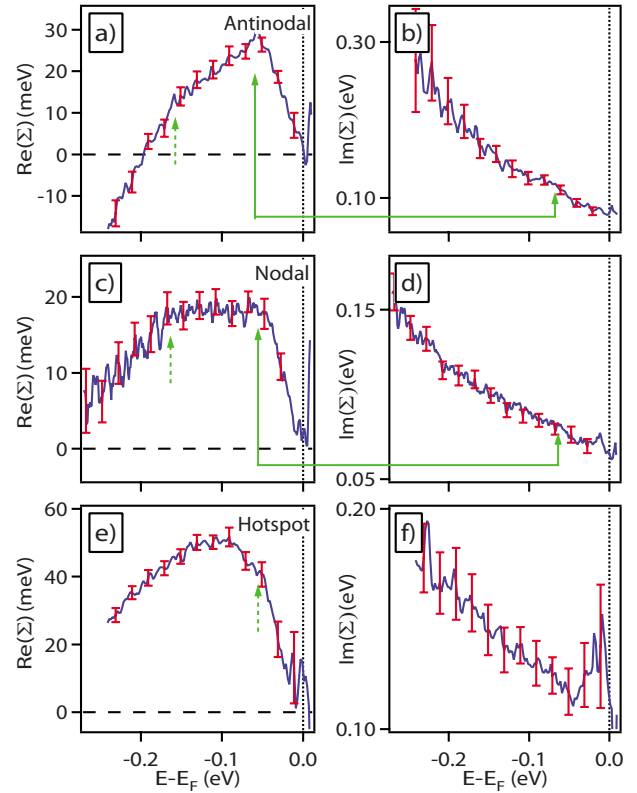

FIG. 2. (Color online) Self-energies extracted from the [(a), (b)] antinodal, [(c), (d)] nodal, [(e), (f)] near-hot spot cuts shown in Fig. 1, respectively. (a), (c), and (e) show the respective real part; (b), (d), and (f) the respective imaginary part. Changes in Re Σ and their corresponding drops in Im Σ are marked by green (gray) arrows. The error bars at selected points represent the 3σ confidence levels from the MDC-Lorentzian fit position in the Re Σ graphs, and the MDC-Lorentzian fit half width at half maximum in the Im Σ graphs. The dashed arrows mark weak changes in Re Σ that are hard to distinguish from the statistical background.

The real and imaginary parts of the self-energy are displayed in Figs. 2(a)–2(f). A peak in Re Σ is clearly visible at 60 ± 5 meV in the antinodal region [Fig. 2(a)], with a corresponding drop at about the same energy in Im Σ [Fig. 2(b)], as expected from causality arguments. Likewise, in the nodal region a plateau is observed at about 50 ± 10 meV in Re Σ [Fig. 2(c)]. The drop in Im Σ [Fig. 2(d)] is much less clear, but the data seem qualitatively consistent with the Kramers-Kronig relations. The difference in our ability to extract the real and imaginary parts of the self-energy can easily be understood from the fact that, for a relatively broad feature, it is much easier to determine its position than width.

We believe the reason why we are now able to resolve the kink in the nodal region and not before[5] is mainly due to the improvement of the momentum resolution. The photon energy (16.75 eV) we used as compared to that used in previous measurements (53 eV) doubles our resolution in k space. Indeed, the line width—which depends significantly on sample quality and resolution—is smaller [cf. Figs. 2(b) and 2(d)] in our data presented in this Rapid Communication.

A change in slope can also be seen in Re Σ near the hot spot region [Fig. 2(e)] around 50 ± 10 meV. However, the
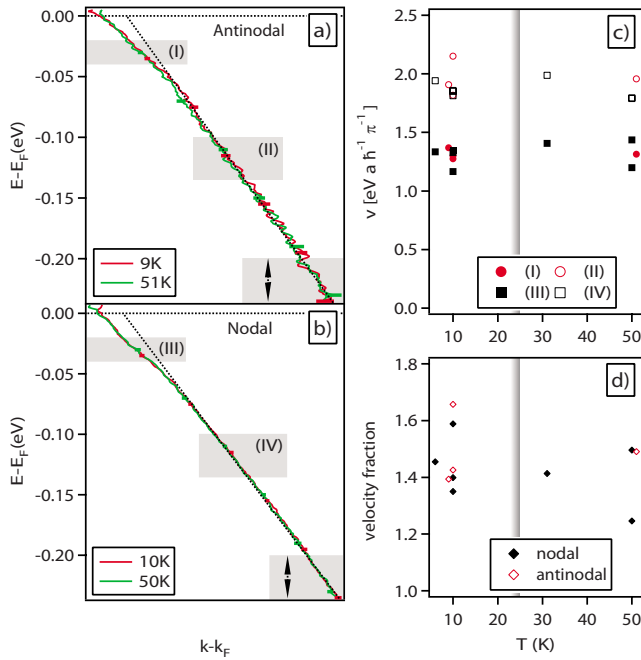
FIG. 3. (Color online) Temperature dependence of the MDC-derived dispersions in the (a) antinodal and (b) nodal regions, with 3σ errors from the fit (thick horizontal bars). The black dotted lines serve as guide to the eye. The data have been average subtracted in the gray region (dotted arrow) to overlay them. (c) Temperature dependent velocities in both nodal and antinodal regions above and below the kink energy, extracted from gray regions indicated by I-IV in (a) and (b). (d) Temperature dependent fractions of the respective velocities below and above the kink energy for the nodal and antinodal regions. T_C is indicated in (c) and (d) (vertical gray line).

relation of its cause to the features in the nodal and antinodal regions remains speculative, even though we find its appearance at the same energy suggestive.

Lastly, a weak change of slope at a higher energy of around 160 meV can be observed in Re Σ in both the nodal and antinodal regions [Figs. 2(a) and 2(c)]. Within the statistics of the data, no change is visible in either of the corresponding Im Σ [Figs. 2(b) and 2(d)] at this energy. It is currently being investigated and will not be discussed here.

The temperature dependence of the observed ubiquitous feature in the nodal and the antinodal regions is shown in Fig. 3. Within the statistics, there is no change visible in either region below (<6 K, 10 K) and above (30 K, 50 K) the SC transition.

For further clarification, the velocities obtained by linear fits against the MDC Lorentz position above (−40 meV $< E - E_F < $−20 meV) and below (−135 meV $< E - E_F < $−100 meV) the renormalization are graphed versus temperature for both nodal and antinodal regions in Fig. 3(c). The data result from seven different measurements on four samples in the nodal, and four different measurements on three samples in the antinodal region. First, neither of these velocities change appreciably across the SC transition. Second, the Fermi velocities of the nodal and antinodal regions are the same, confirming previous results.[5] Third, the ratio of renormalized and unrenormalized velocities—which are in-
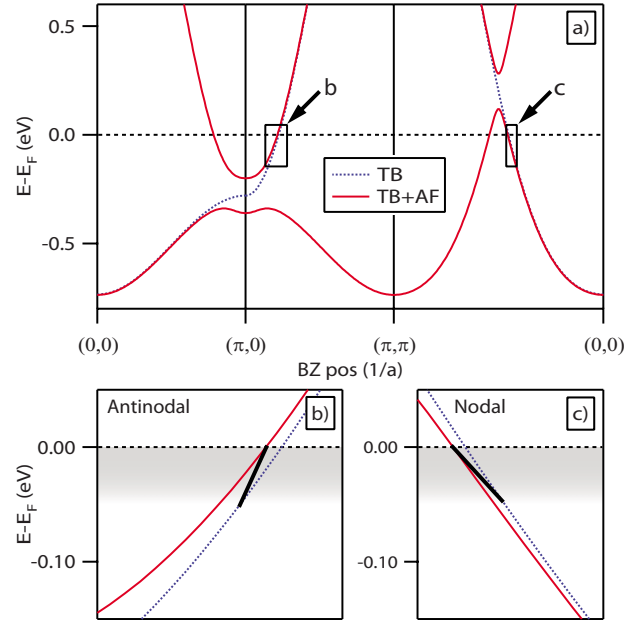

FIG. 4. (Color online) Schematic tight-binding (TB) models. Solid blue (black) curves correspond to TB without, dotted red (black) ones to TB with simple perturbative $V_{\pi,\pi}$ scattering. (a) Cuts along high-symmetry directions in the BZ. (b) Antinodal and (c) nodal details of (a). The enlarged regions shown in (b) and (c) are indicated by rectangles in (a).

dicative of the renormalization strength of the electronic band—do not seem to change within the statistics in both nodal and antinodal regions, cf. Fig. 3(d).

The n-doped HTSCs possess hot spots that lie on the AF BZ boundary,[3,5] and recently, pockets were observed suggesting a band back folding at the AF BZ boundary,[14] a possible mechanism could be (π, π) scattering due to some short-range or remnant antiferromagnetic (spin density wave) ordering. To first order, this folding results in a pair of new band sheets [cf. Fig. 4(a)].[15] Whenever there is a crossover from one folded band sheet to another, as for example at $(\pi, 0)$ in the antinodal region (solid curve to solid curve in Fig. 4), one expects a kinklike feature in the dispersion. We do not, however, think that this is the sole cause for the low-energy feature, since this crossover takes place at the band bottom ($\approx$300 meV) in the antinodal region and above the Fermi energy in the nodal region, leading to a highly anisotropic behavior both in shape and energy of the feature, contradicting our observed isotropy in both energy and renormalization strength.

If we were to invoke an electron energy dependence of the scattering, $V_{\pi,\pi}(\omega_k)$, whereas the interaction is nonzero only for $|\omega_k| < \omega_{max} \approx 50$ meV, a fadeover is produced between the unrenormalized, unfolded band (dotted curve in Fig. 4) and one of the renormalized, folded bands [solid curves; cf. Figs. 4(b) and 4(c)] around ω_{max}. However, we do not know of any interaction with above-mentioned energy dependence. Provided it exists, the produced crossover results in a downward kink in the nodal region and an *upward* kink in the antinodal region, contradicting our observations.

We also argue against a magnetic resonance or spin-flip

waves as the origin of the low-energy renormalization we discuss here, since the characteristic energy scales for electron-doped cuprates are too different from the 55 meV observed by us. First, the relevant region of the spin excitation dispersion relation is about 0.3 eV.[16] Second, a resonance has been reported at about 10 meV in PLCCO (Ref. 17) and in NCCO.[18] This is still disputed; at least for NCCO, recent data show even lower energy scales (within 4–8 meV) for the SC gap and a possible resonance.[19] Whether a more complicated interaction mechanism could explain our data is to be investigated.

A phononic origin on the other hand could account for the isotropy of the renormalization strength and energy of the kink observed by us in a simple picture (although more intricate phononic interactions may result in anisotropic renormalizations[20,21] and even *d*-wave SC gaps[20,22]). Furthermore, a softening with doping of oxygen phonon modes in the relevant energy regime has been observed via inelastic x-ray scattering[23] and inelastic neutron scattering.[24] Raman and IR spectra also show the existence of oxygen modes of the relevant energies.[25] In addition, the fact that the kink at both nodal and antinodal regions does not change across the SC transition lends further support to the electron-phonon coupling scenario. The absence of a change of the kink energy across the superconducting phase transition is due to the small superconducting gap in NCCO. Also, the EDCs at the E_F crossing exhibit the same structure as in Bi2201—a small

peak near E_F and a shallow dip at the same energy of the renormalization seen in Re Σ [cf. Figs. 1(b) and 1(d)].[11]

Within the context of electron-phonon interaction, a renormalization at around 70 meV is seen in the nodal region of *p*-doped HTSCs in ARPES and has been attributed to electron-phonon interactions.[10,26] A softening of an oxygen mode was seen as well for the *n*-doped compound NCCO via inelastic neutron and x-ray scattering (55 meV),[23,27] and now also in the nodal region via ARPES as observed by us in the same relevant energy region. Independently, Park *et al.*[28] and Liu *et al.*[29] discovered a kink in the nodal region in several *n*-doped HTSCs and came to very similar conclusions regarding its origin.[30] If interpreted as due to electron-phonon coupling, our results suggest that electronic coupling to the oxygen phonon mode may be even more universal, now stretching across the phase diagram. We speculate that these phonon modes may play a vital role in determining the low-energy physics of the HTSCs.[20,22]

[1] Y. Tokura, H. Takagi, and S. Uchida, Nature (London) **337**, 345 (1989).

[2] H. Matsui, K. Terashima, T. Sato, T. Takahashi, S.-C. Wang, H.-B. Yang, H. Ding, T. Uefuji, and K. Yamada, Phys. Rev. Lett. **94**, 047005 (2005).

[3] N. P. Armitage *et al.*, Phys. Rev. Lett. **87**, 147003 (2001).

[4] N. P. Armitage *et al.*, Phys. Rev. Lett. **88**, 257001 (2002).

[5] N. P. Armitage *et al.*, Phys. Rev. B **68**, 064517 (2003).

[6] K. Yamada, K. Kurahashi, T. Uefuji, M. Fujita, S. Park, S.-H. Lee, and Y. Endoh, Phys. Rev. Lett. **90**, 137004 (2003).

[7] E. M. Motoyama, G. Yu, I. M. Vishik, O. P. Vajk, P. K. Mang, and M. Greven, Nature (London) **445**, 186 (2007).

[8] P. Li, K. Behnia, and R. L. Greene, Phys. Rev. B **75**, 020506(R) (2007).

[9] Y. Dagan, M. M. Qazilbash, C. P. Hill, V. N. Kulkarni, and R. L. Greene, Phys. Rev. Lett. **92**, 167001 (2004).

[10] A. Damascelli, Z. Hussain, and Z.-X. Shen, Rev. Mod. Phys. **75**, 473 (2003).

[11] A. Lanzara, P. V. Bogdanov, X. J. Zhou, N. Kaneko, H. Eisaki, M. Greven, Z. Hussain, and Z. X. Shen, J. Phys. Chem. Solids **67**, 239 (2006).

[12] E. M. Motoyama, P. K. Mang, D. Petitgrand, G. Yu, O. P. Vajk, I. M. Vishik, and M. Greven, Phys. Rev. Lett. **96**, 137002 (2006).

[13] A. Kaminski, M. Randeria, J. C. Campuzano, M. R. Norman, H. Fretwell, J. Mesot, T. Sato, T. Takahashi, and K. Kadowaki, Phys. Rev. Lett. **86**, 1070 (2001).

[14] S. R. Park, Y. S. Roh, Y. K. Yoon, C. S. Leem, J. H. Kim, B. J. Kim, H. Koh, H. Eisaki, N. P. Armitage, and C. Kim, Phys. Rev. B **75**, 060501(R) (2007).

[15] N. P. Armitage, Ph.D. thesis, Stanford University, 2001.

[16] S. D. Wilson, S. Li, H. Woo, P. Dai, H. A. Mook, C. D. Frost, S. Komiya, and Y. Ando, Phys. Rev. Lett. **96**, 157001 (2006).

[17] S. D. Wilson, P. Dai, S. Li, S. Chi, H. J. Kang, and J. W. Lynn, Nature (London) **442**, 59 (2006).

[18] J. Zhao, P. Dai, S. Li, P. G. Freeman, Y. Onose, and Y. Tokura, Phys. Rev. Lett. **99**, 017001 (2007).

[19] G. Yu, Y. Li, E. M. Motoyama, K. Hradil, R. A. Mole, and M. Greven, arXiv:0803.3250 (unpublished).

[20] Z. X. Shen, A. Lanzara, S. Ishihara, and N. Nagaosa, Philos. Mag. B **82**, 1349 (2002).

[21] T. P. Devereaux, T. Cuk, Z.-X. Shen, and N. Nagaosa, Phys. Rev. Lett. **93**, 117004 (2004).

[22] D. M. Newns and C. C. Tsuei, Nature (London) **3**, 184 (2007).

[23] M. d'Astuto, P. K. Mang, P. Giura, A. Shukla, P. Ghigna, A. Mirone, M. Braden, M. Greven, M. Krisch, and F. Sette, Phys. Rev. Lett. **88**, 167002 (2002).

[24] H. J. Kang, P. Dai, D. Mandrus, R. Jin, H. A. Mook, D. T. Adroja, S. M. Bennington, S.-H. Lee, and J. W. Lynn, Phys. Rev. B **66**, 064506 (2002).

[25] A. P. Litvinchuk, C. Thomsen, P. Murugaraj, E. T. Heyen, and M. Cardona, Phys. Rev. B **43**, 13060 (1991).

[26] A. Lanzara *et al.*, Nature (London) **412**, 510 (2001).

[27] M. Braden, L. Pintschovius, T. Uefuji, and K. Yamada, Phys. Rev. B **72**, 184517 (2005).

[28] S. R. Park, D. J. Song, C. S. Leem, C. Kim, C. Kim, B. J. Kim, and H. Eisaki, arXiv:0808.0559 (unpublished).

[29] H. Liu *et al.*, arXiv:0808.0802 (unpublished).

[30] We can not, however, currently confirm the feature at ≈ 23 meV in the nodal region observed by Liu *et al.*